Arabian Journal of Chemistry (2023) **16**, 104597

King Saud University

Arabian Journal of Chemistry

www.ksu.edu.sa
www.sciencedirect.com

ORIGINAL ARTICLE

Basic characterization and Alzheimer's disease relieving property of a glucose riched polysaccharide from *Cibotium barometz*

Zhonghao Zhang [a], Yujin Wang [a], Tao Gao [a], Zizhong Tang [a], Lijun Zhou [a], Tao Chen [a], Shiling Feng [a], Chunbang Ding [a], Shu Yuan [b], Ming Yuan [a,*]

[a] *College of Life Science, Sichuan Agricultural University, Ya'an 625014, China*
[b] *College of Resources, Sichuan Agricultural University, Chengdu 611130, China*

Received 3 July 2022; accepted 13 January 2023
Available online 20 January 2023

KEYWORDS

Alzheimer's disease;
Cibotium barometz polysaccharide;
Antioxidant;
Aβ

Abstract The water-soluble polysaccharides from plants have attracted ever-increasing attention in the field of food and drug due to their various activities and low toxicity. CBP50-1, as a purified fraction of polysaccharide from the rhizome of *Cibotium barometz* (CBP), mainly consisted of glucose (55.45%) and xylose (25.27%). CBP50-1 showed excellent antioxidant activity for scavenging 2,2 Diphenyl 1 picryl hydrazy (DPPH) radical and hydroxyl radical, further inhibiting lipid peroxidation. CBP50-1 significantly improved the survival rate of *Caenorhabditis elegans* under thermal and oxidative stress. Furthermore, CBP50-1 reduced the paralysis and oxidative damage induced by amyloid-beta (Aβ) and increased the antioxidant enzyme activity in Alzheimer's disease (AD) model *C. elegans* CL4176 through c-Jun *N*-terminal kinase (JNK) mitogen-activated protein kinase (MAPK) signal pathway. Thus, CBP50-1 had a potential application in health industries.

1. Introduction

Alzheimer's disease (AD), or senile dementia, is a progressive chronic degenerative dementia of the central nervous system that occurs majority in the elderly. With the arrival of an aging society, the incidence of AD is increasing year by year. One in every 85 people will live with AD symptoms or a tendency to develop into AD by 2050 (Brookmeyer et al., 2018). The main hypotheses concerning AD include amyloid-beta (Aβ) peptides, dystrophic neuronal extensions, activated microglia, and reactive astrocytes (Folch et al., 2018). Additionally, much evidence proved that free radicals are related to AD (Jiang et al., 2016; Padurariu et al., 2013). The relationship between oxidative damage and amyloid plaques is interactive. Oxidative stress is indirectly involved in the amyloid genesis by inducing intralysosomal accumulation of Aβ (Zheng et al., 2006). Moreover, Aβ disturbed the redox balance and aggravated oxidative damage by precipitating lipid peroxidation and mitochondrial dysfunction, resulting in cell death (Zhou et al., 2014).

There is ample evidence that the intake of antioxidants could improve our resistance to diseases (Ribeiro et al., 2011). Natural polysaccharides showed many biological properties such as anti-

* Corresponding author.
E-mail address: yuanming@sicau.edu.cn (M. Yuan).
Peer review under responsibility of King Saud University.

Production and hosting by Elsevier

https://doi.org/10.1016/j.arabjc.2023.104597
1878-5352

oxidation, anti-aging, anti-tumor, and anti-inflammatory (Mzoughi et al., 2018). Owing to their safety and nontoxic properties, some of these polysaccharides could be antioxidants and drugs (Teng et al., 2020; Zheng et al., 2020). Consequently, there is growing attention to pursuing the isolation, characterization, and bioactivity of diverse polysaccharides from natural materials because of their potential application in functional food and medicine. *Caenorhabditis elegans* is often used to evaluate the activity of polysaccharides due to its short lifespan and easy operation (Feng et al., 2018; Zhang et al., 2018). *C. elegans* CL4176 expressed the human $A\beta_{1-42}$ in the muscle when the culture temperature was over 23 °C, which caused progressive paralysis (Yen et al., 2021). This type of worm is often used to evaluate the effects of polysaccharides on AD (Li et al., 2018; Lin et al., 2020).

Cibotium barometz (L.) J. Sm, a great fern up to 2 meters, is widely distributed in Guangdong, Guangxi, Guizhou, Sichuan, and Yunnan in China (Zhang and Nishida,2013). It is a traditional food because of its abundant starch in the rhizome, and it is also a Chinese medicinal herb to relieve rheumatic arthralgia and cure traumatic hemorrhage (Huang et al., 2018). It is widely used as an ornamental plant today. Decoction was the most convenient method to obtain its effective constituents. Therefore, the polysaccharide was considered an active ingredient in the *Cibotium barometz* rhizome. It showed excellent immunoactivity and antioxidant properties *in vitro* (Huang et al., 2018; Shi et al., 2020). Previous research on fern polysaccharides mainly aimed at the extraction method or preliminary analysis of its antioxidant activity (Chiang and Lai, 2019; Xu et al., 2009). There was little report about its mitigation effect on AD. Based on the close relationship between oxidative damage and amyloid plaques, we evaluated the potential of polysaccharide from *Cibotium barometz* to relieve the oxidative damage and symptoms of paralysis in the AD model of *C. elegans*.

2. Materials and methods

2.1. Material and reagents

The *C. barometz* rhizome was purchased from Guangxi in China. The dried rhizome was pulverized and screened through 80-mesh sieves. Absolute ethyl alcohol, sodium chloride, *n*-butyl alcohol, chloroform, acetone, Ascorbic acid (Vc), Congo red, ethyl ether, and $K_2S_2O_4$ were obtained from Chengdu Kelong Chemical CO., ltd (Chengdu, China). Monosaccharide standards, 2,2 Diphenyl 1 picryl hydrazy (DPPH) were purchased from Solarbio Sci. & Tech. Co., ltd. (Beijing, China). All reagents were analytically pure.

2.2. Caenorhabditis elegans strains maintenance and treatment

Wild type N_2 and CL4176 (*pAF29(myo-3/A-Beta 1–42/let UTR) + pRF4 rol-6 (su1006)*) were kept at 20 °C and 16 °C, respectively. All strains were cultured with *Escherichia coli* var. OP50 and maintained on standard nematode growth medium plates with CBP50-1 or not.

2.3. Optimation for polysaccharide extraction

2.3.1. Single-factor experiment

The effects of extraction time (30–70 min), ultrasonic power (150–270 W), extraction temperature (30–70 °C), and liquid to solid ratio (15–35 mL/g) on the yield of CBP were evaluated. The sugar content was assayed according to Zhao et al. (2019). The extraction yield was calculated by the formula:

$$Extractionyield = C \times V/M \times 100 \quad (1)$$

where C was the sugar content (mg glucose/mL); V was the volume (mL), and M was the sample dry weight (g DW).

2.3.2. Design of response surface methodology (RSM)

The design of RSM and statistical analysis were done by Design Expert Software (8.0.6). with each parameter at three levels: high (+1), medium (0), and low (-1). The Box-Behnken design (BBD) for the extraction of CBP were shown in Table S1. Each experiment was performed three times and the mean was taken as the response. Analysis of experimental data was performed using analysis of variance (ANOVA) and the results were fitted by the following full second-order polynomial equation:

$$Y = \beta_0 + \sum_{i=1}^{4} \beta_i X_i + \sum_{i=1}^{4} \beta_{ii} X_i^2 + \sum_{j<i}^{3} \sum_{i=1}^{4} \beta_{ij} X_i X_j \quad (2)$$

where Y is the predicted response (extraction yield), A_i and A_j are the coded independent variables, and β_0, β_i, β_{ii}, and β_{ij} are the regression coefficients of variables for intercept, linear, quadratic, and interaction terms, respectively.

2.3.3. Extraction and purification of polysaccharides

The degreased sample (200 g) was extracted under the optimized condition. The supernatant was condensed with a rotary evaporator, and the same volume of anhydrous ethanol was added, centrifuging and collecting the precipitates (CBP50). After freeze-drying, the crude polysaccharides were collected. Seveg solution was used for deproteinization. Deproteinated polysaccharides (CBP50) were separated by anion-exchange chromatography (DEAE-52 cellulose column, 2.5 × 30 cm) and eluted with 0–0.5 mol/L NaCl. The fraction washed with deionized water was named CBP50-1, and further purified with a Sephadex G-200 column. Then, followed by dialyzing (3500 Da) and lyophilizing, purified CBP50-1 was obtained.

2.4. Assay of total sugars, uronic acid, and protein

The uronic acid content and protein content were determined according to Zhao et al. (2019). The total sugar content was determined according to Zhao et al. (2019).

2.5. Characterization of CBP50-1

2.5.1. Molecular weight and monosaccharide composition

The molecular weight of CBP50-1 was determined by High-performance Gel Chromatography, and the standards curve was made with a series of dextrans.

The monosaccharide of CBP50-1 was determined through Agilent 1260 High-performance Liquid Chromatography (HPLC) system (Agilent, Santa Clara, CA, USA) coupled with an Agilent C-18 column (Ø 4.6 × 250 mm, 5 μm) (Wang et al., 2015). 0.05 mol/L phosphate buffer solution (pH 6.7) and acetonitrile worked as mobile phase with a 1.0 mL/min flow rate. The detection wavelength was 254 nm with the DAD detector.

2.5.2. The UV spectroscopy analysis and FT-IR

UV–visible absorption of CBP50-1 (100 μg/mL) was recorded with a spectrophotometer (Shimadzu UV-1800, Japan). CBP50-1 was compressed into a KBr pellet and scanned with FTIR-8400S (Shimadzu, Japan).

2.5.3. Thermal properties

Thermal properties were determined with a Q20 differential scanning calorimeter (DSC) (AT, USA) under N_2 at 0.1 MPa. 3.0 mg of CBP50-1 was placed in a closed aluminum pan and heated from 50 to 350 °C.

2.5.4. Congo red assay

Congo red (1 mL, 0.2 mmol/L) and polysaccharide solution (1.5 mL, 2.0 mg/mL) were mixed, then 2 mol/L NaOH was added to the final concentration of 0–0.5 mol/L, followed by incubation for 30 min. The solution was scanned with a spectrophotometer (400–700 nm) (Shimadzu UV-1800 Japan).

2.6. Antioxidant activities in vitro

Hydroxyl radical scavenging activity and DPPH radical scavenging activity was performed as Zhao et al. described (2019), and Vc was taken as control. anti-lipid-peroxidation capacity was measured as Liu & Huang described (Liu and Huang, 2018), and 2,6-Di-*tert*-butyl-p-cresol (BHT) worked as a control.

2.7. Thermal stress and oxidative stress of N_2

Synergized nematodes were cultured after lysis. The nematodes of the L4 stage were randomly transferred to new plates (containing 0.1 mg/mL CBP50-1 or not). For thermal stress, 30 nematodes were exposed to 35 °C and the survival worms were counted after 14 h. For oxidative stress, 30 nematodes were transferred onto a 24-well plate with 50 μmol/L of Juglone in 500 μL S-medium per well. The survival worms were counted after 20 h.

2.8. Determination of paralysis rate

Synchronized L3 larvae (CL4176) were treated with 0.1 mg/mL CBP50-1 for 48 h at 16 °C and then transferred to 25 °C. The number of paralysis nematodes was recorded after 36 h. Every plate contained 40 nematodes.

2.9. Fluorescent staining of Aβ deposits in C. elegans strain

Synchronized L3 larvae CL4176 was treated with 0.1 mg/mL CBP50-1 for 36 h at 16 °C and then transferred to 25 °C for 36 h. The fluorescent staining of Aβ deposits in CL4176 was performed according to Wang et al. (2022).

2.10. Measurement of antioxidant enzyme activity and MDA level

Synchronized L3 larvae CL4176 was treated with 0.1 mg/mL CBP50-1 for 36 h at 16 °C and then transferred to 25 °C for 36 h. Antioxidant enzyme activity superoxide dismutase (SOD) and catalase (CAT) and malonaldehyde (MDA) content were determined with corresponding kits (Nanjing, Jiancheng Cot).

2.11. Quantitative real-time PCR (qRT-PCR)

Total RNA was extracted using the RNA simple Total RNA Kit, and the quality and quantity of RNA were assessed with Nanodrop ND-1000 (NanoDrop Technologies Wilmington, DE) and formaldehyde gel electrophoresis. cDNA was synthesized following the RrimeScript TMRT regent kit's instructions. Quantitative Real-Time PCR was performed on the CFXTM96 Real-time system (BIO-RAD, California, USA) following the instructions of the SYBR Premix Ex Taq kit. The PCR protocol was as follows: 95 °C for 2 min and then 45 cycles of 95 °C for 5 s, 55 °C for 10 s, and 72 °C for 20 s. The results were evaluated using the $2^{-\Delta\Delta CT}$ method relative to Actin. Primer information is shown in Table. S2.

2.12. Statistical analysis

All analyses were done with SPSS 22.0. All the experiments were conducted three times independently. Data were presented as the mean ± standard error of the mean (SEM). $P < 0.05$ was regarded as significant.

3. Results

3.1. Effect of single-factors on the yield of CBP

To measure the influence of ultrasonic power (150, 180, 210, 240, and 270 W) on the yield of CBP, the extraction temperature was 50 °C, the extraction time was 50 min, and the ratio of liquid to solid was 25 mL/g. Polysaccharide yield increased with ultrasonic power, and it came up to the maximum when the power was 210 W. Subsequently, the yield dropped with the power (Fig. S1 A). Therefore, 210 W was selected as the optimum ultrasonic power.

When evaluating the impact of extraction times (30, 40, 50, 60, and 70 min) on the yield of CBP, the temperature was 50 °C, the ultrasonic power was 210 W, and the ratio of liquid to sample was 25 mL/g. The yield kept escalating with the extraction time, and it reached the maximum when the time was 60 min (Fig. S1 B). Subsequently, the yield exhibited a slight decline. Hence, 60 min was chosen for optimum.

To assess the effect of the extraction temperature (30, 40, 50, 60, and 70 °C) on the yield of CBP, the ultrasonic power, time, and the ratio of liquid to solid were followed by 210 W, 50 min, and 25 mL/g. The yield reached the maximum when the temperature was 60 °C, then it declined with the temperature (Fig. S1 C). Thus, 60 °C was chosen for optimum.

When appraising the influence of the solvent to the material ratio (15, 20, 25, 30, and 35 mL/g) on the CBP yield, the ultrasonic power, time, and extraction temperature were followed by 210 W, 50 min, and 50 °C. The CBP yield increased with the ratio, and it reached the maximum when the ratio was 25 mL/g (Fig. S1 D). The redundant solvent increased the diffusion distance of compounds from sample tissue to liquid and inhibited their dissolution (Shang et al., 2020). Accordingly, 25 mL/g was adopted for further optimum.

3.2. Optimization of CBP extraction condition by Box-Behnken design

3.2.1. The RSM model fitting

According to the experimental conditions given by the BBD design, the corresponding yield was presented in Supplementary material Table S1. The simulated model was shown in the following equation:

$$Y = 8.62 + 0.39 \times A_1 - 0.01 \times A_2 + 0.19 \times A_3 + 0.29 \times A_4 + 0.077 \times A_1A_2 + 0.52 \times A_1A_3 - 0.60 \times A_1A_4 + 0.53 \times A_2A_3 + 0.44 \times A_2A_4 + 0.31 \times A_3A_4 - 0.32 \times A_1^2 - 0.17 \times A_2^2 - 0.58 \times A_3^2 - 0.66 \times A_4^2$$

Where A_1 is the ultrasonic power, A_2 is time, A_3 is temperature, A_4 is the ratio of liquid to solid, and Y is the yield of CBP.

The Model F (11.05) and P (<0.05) implied the model was reliable. In this case, the P of two linear terms (A_1, A_3, and A_4), four interactive terms (A_1A_3, A_1A_4, A_2A_3, A_2A_4, and A_3A_4), and two quadratic terms (A_1^2, A_3^2, and A_4^2) were lower than 0.05, suggesting these parameters significantly affected the yield of CBP. The P (1.20) of "Lack of Fit" was not appreciable, which is consistent with Model F. These results suggested that the model could guide the experimental design (Table S1).

The "R^2" (0.92) was not close to the "Adj R^2" (0.83). This might be caused by the low interaction between the ultrasonic power and extraction time as well as extraction temperature and the ratio of liquid to sample. The interactions between ultrasonic power and temperature, ultrasonic power and the ratio of liquid to sample, temperature and time, and time and the ratio of liquid to sample were notable (Fig. S2). These results were consistent with the ANOVA analysis (Table S1).

3.2.2. Overall optimization and model verification

Based on the model equation, the optimum variables for CBP extraction were followed by 26.5 mL/g of liquid to solid ratio, 67.6 °C of temperature, 69.6 min of time, and 238.5 W of ultrasonic power, and the maximum yield of CBP was 97.4 mg glucose/g DW. For operation convenience, the proved experiment was done under the 26.5 mL/g of liquid to solid ratio and 240 W of ultrasonic power at 68 °C for 70 min. The actual yield of CBP was 95.91 ± 1.33 mg glucose/g DW, which was very similar to the predicted yield, suggesting the model was suitable for CBP extraction.

3.3. Physicochemical properties

The CBP was precipitated by 50 % ethanol and named CBP50. CBP50 was fractioned with DEAE-52 and then CBP50-1 (eluted by water) was further purified with Sephadex G-200 (Fig. S3). Its molecular weight was 61.02 KDa (Fig. S4), and it contained 89.67 % of sugar. CBP50-1 contained 1.89 % of protein and had no uronic acid.

The polysaccharide CBP50-1 mainly contained glucose (55.45 %) and xylose (25.27 %), along with arabinose (7.30 %), fucose (6.36 %), mannose (3.67 %), and rhamnose (1.95 %) (Fig. 1). The kind of monosaccharide was agreed with previous reports (Huang et al., 2018; Shi et al., 2020), and the difference in the proportion of each monosaccharide might due to the different origin and extraction treatment of the *C. barometz* rhizome.

3.4. The FT-IR and thermogravimetric analysis of CBP50-1

The FT-IR spectrum could provide information about the vibrations of atoms or functional groups in molecules, which is extensively used in the qualitative analysis of complex compounds. As shown in Fig. 2A, the bond at 3419 cm^{-1} was

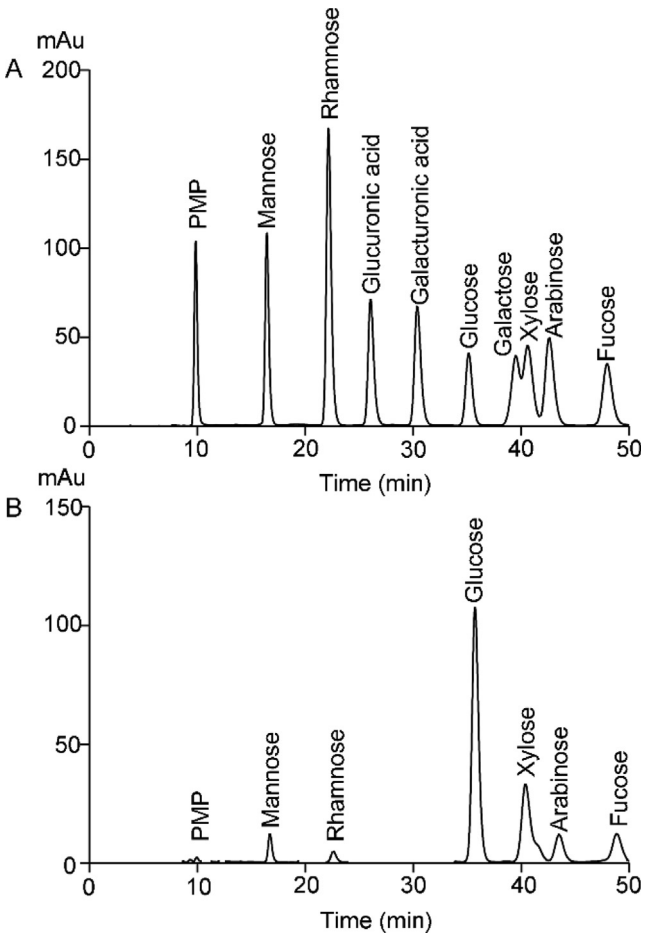

Fig. 1 Monosaccharide composition of CBP50-1. (A) Standard monosaccharides. (B) Monosaccharides composition of CBP50-1.

O—H, and the bond at 2937 cm^{-1} was C—H in the sugar ring. The peaks at 1611 cm^{-1} and 1417 cm^{-1} were attributed to the hydration peak. The band at 1253 cm^{-1} was the C—O—C bonds in acetyl esters and 1072 cm^{-1} was the C—O—H (Mzoughi et al., 2018). The characteristic peak at 894 cm^{-1} suggested the existence of a β-D-glucose pyranosyl ring in CBP50-1.

The differential thermogravimetry (DTG) curve of CBP50-1 was determined by TGA (Fig. 2B). A slight peak occurred at 152.50 °C due to the release of water from CBP50-1. Subsequently, an endothermic peak appeared at 182.38 °C indicted the exothermic decomposing and oxidation of the polysaccharides (Yu et al., 2019). Besides, the presence of an exothermic peak at 261.45 °C might be caused by the high thermal depolymerization and debranching of CBP50-1.

3.5. Congo red analysis and UV spectral of CBP50-1

The maximum absorption wavelength (λ_{max}) change of polysaccharide and Congo red-complex in an alkaline solution could provide information about polysaccharide conformation. When Congo red forms a complex with a three-helix polysaccharide, the λ_{max} will change. While NaOH exceeded 0.3 mol/L, its λ^{max} decreased rapidly (Zhao et al, 2019). The λ_{max} of control dropped with the concentration of the alkaline solution. The λ_{max} of the mixture of Congo red and CBP50-1

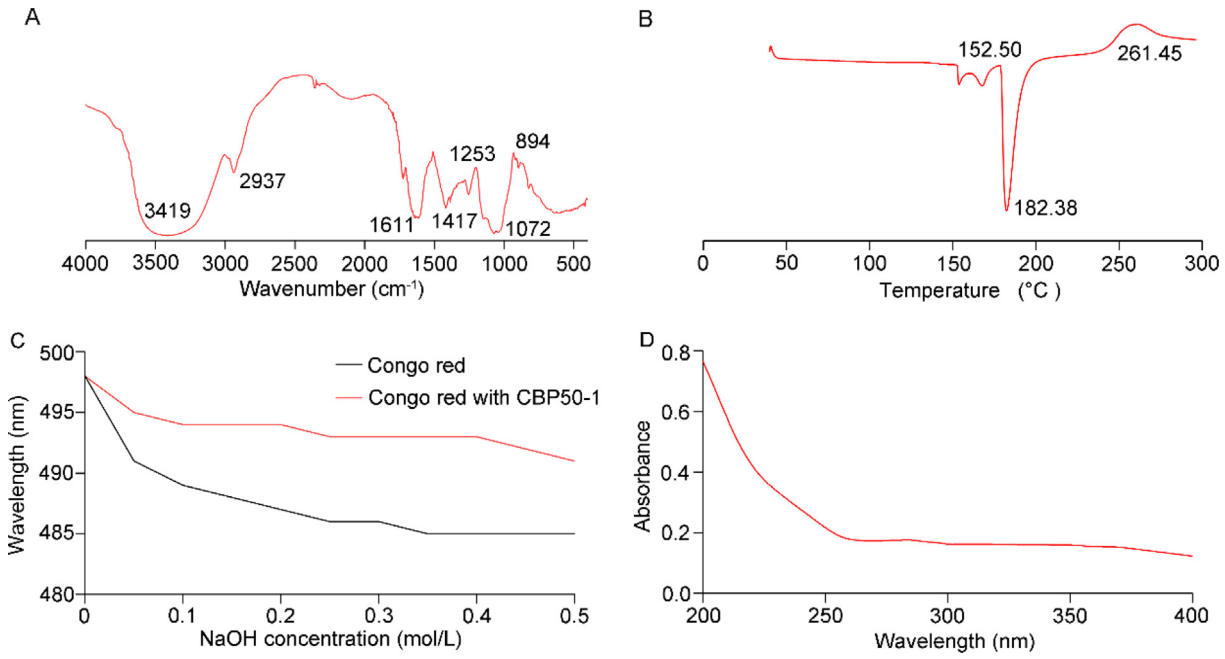

Fig. 2 The property of CBP50-1. (A) FT-IR spectrum of CBP50-1. (B) Thermogravimetric analysis. (C) Congo red of CBP50-1. (D) UV spectrum of CBP50-1.

showed the same tendency, indicating that CBP50-1 had no three-helix conformation (Fig. 2C).

No apparent peak occurred at 260 or 280 nm (Fig. 2D), suggesting CBP50-1 contained little nucleic acid and protein. This result confirmed the previous quantitative analysis of protein (3.3).

3.6. Antioxidant activity in vitro

Under normal physiological conditions, reactive oxygen species (ROS) are balanced by antioxidative defense systems. Once ROS overwhelms the cellular antioxidant system and causes oxidative damage, a series of untoward effects even neu-

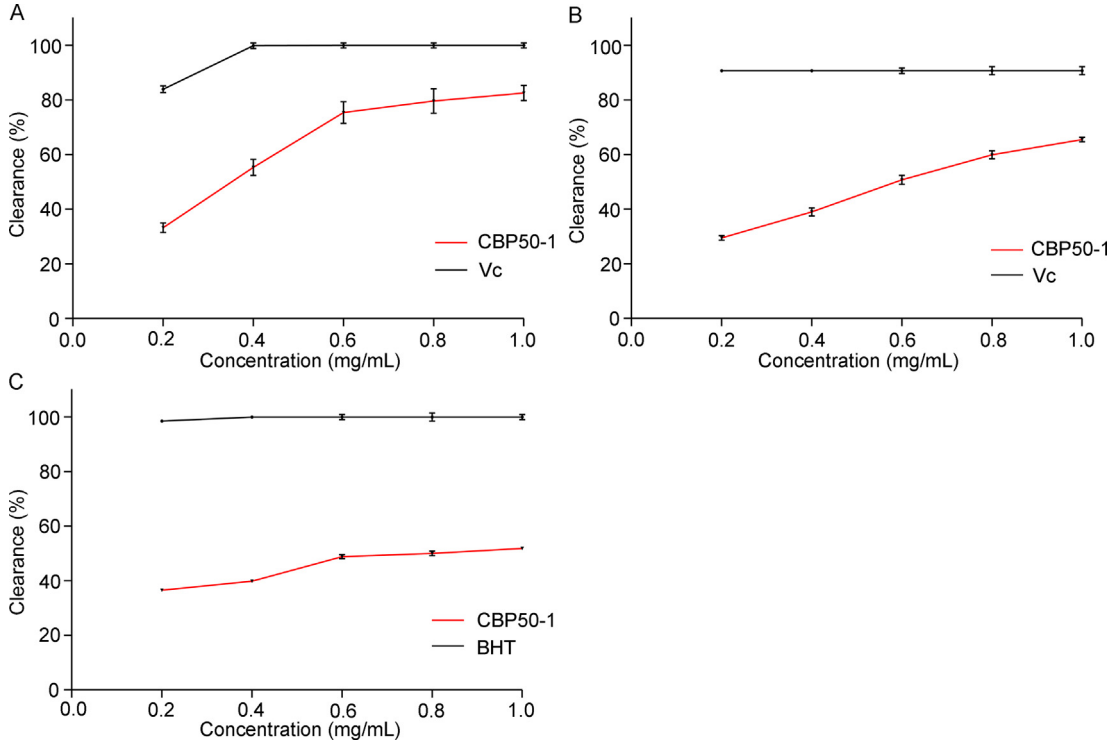

Fig. 3 Antioxidant activity of CBP50-1. (A) DPPH radical cleaning activity. (B) hydroxyl radical cleaning activity. (C) anti-lipid peroxidation capacity.

ron destruction occurs (Jiang et al., 2016). CBP50-1 showed a remarkable DPPH cleaning activity. It reached 82.57 % of the clearance rate at 1.0 mg/mL (Fig. 3A). Its hydroxyl radical scavenging rate was 65.51 % at 1.0 mg/mL (Fig. 3B). Additionally, CBP50-1 also showed strong anti-lipid-peroxidation capacity and its inhibition rate of lipid peroxidation was 51.83 % at 1.0 mg/mL (Fig. 3C).

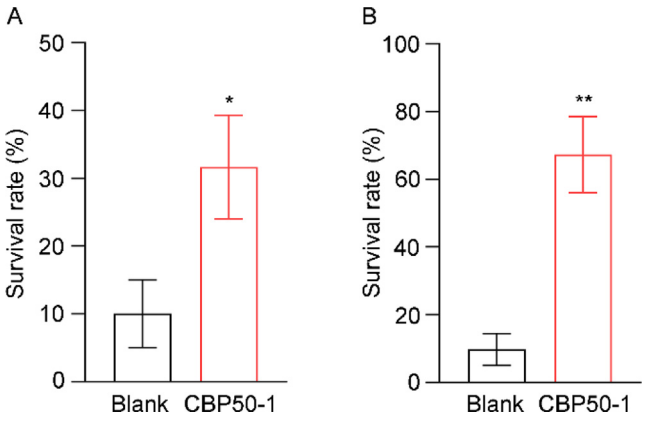

Fig. 4 Effects of CBP50-1 on thermal stress and oxidative stress in N_2. (A) Thermal stress. (B) Oxidative stress (* is significant at the 0.05 level, ** is significant at the 0.01 level).

3.7. Polysaccharide CBP50-1 improved the survival rate of N_2 under heat and oxidative stress

The survival rate of the CBP50-1-treated worms was higher than the control under heat stress as well as acute oxidative stress (Fig. 4), indicating that CBP50-1 could improve the tolerance of N_2 under adverse conditions. Other polysaccharides also played a similar role in N_2 (Gu et al., 2020; Wang et al., 2019). Many pieces of research proved that oxidation was the main damage caused by heat stress (Hamilton et al., 2016; Kaldur et al., 2014). Therefore, CBP50-1 might be a good antioxidant in N_2.

3.8. Polysaccharide CBP50-1 relieved symptoms of paralysis and oxidative damage induced by Aβ in C. Elegans CL4176

Although the exact mechanism of AD has not been elucidated, Aβ was considered one of the major risk factors. It is effective for the treatment of AD by reducing or eliminating the nega-

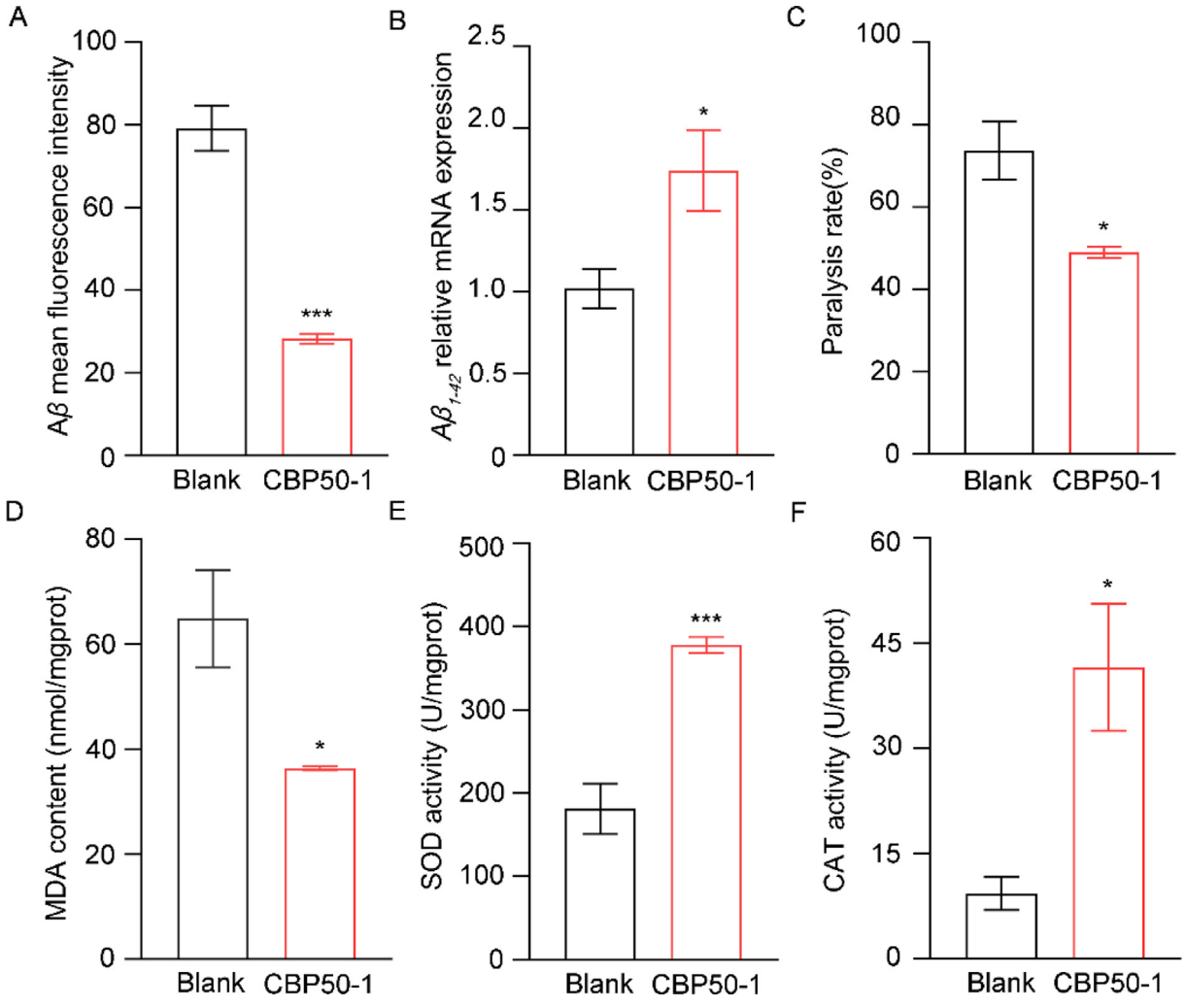

Fig. 5 Effects of CBP50-1 on C. elegans CL4176. (A) Aβ deposits mean fluorescent intensity. (B) $A\beta_{1\text{-}42}$ relative mRNA expression. (C) Paralysis rate. (D) MDA accumulation. (E) SOD activity. (F) CAT activity (* is significant at the 0.05 level, *** is significant at the 0.001 level).

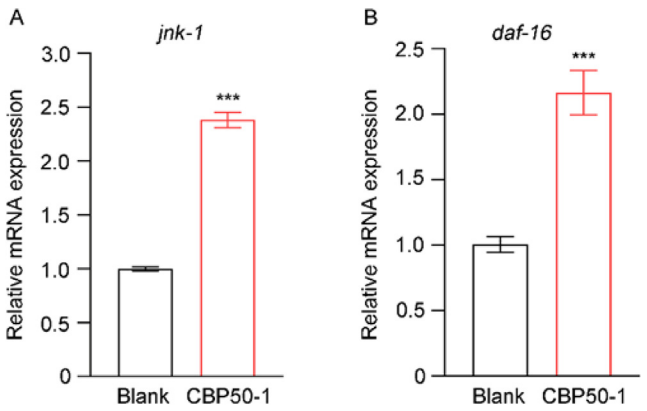

Fig. 6 Relative mRNA expression. (A) *jnk-1* expression. (B) *daf-16* expression (*** is significant at the 0.001 level).

tive consequences of Aβ (Sun et al., 2015). The expression of $A\beta_{1\text{-}42}$ in the CBP50-1 group was higher than blank, but the mean fluorescent intensity was lower compared to the blank (Fig. 5A, B). These results indicated that CBP50-1 reduced the accumulation of $A\beta_{1\text{-}42}$ in CL4176, which suggested CBP50-1 might work at the translational or posttranslational level. Besides, CBP50-1 could reduce the paralysis rate and the accumulation of MDA induced by Aβ (Fig. 5C, D).

Growing evidence indicated that Aβ-induced neurotoxicity was closely related to oxidative damage (Padurariu et al., 2013). Aβ induces oxidative damage to DNA, proteins, and lipids, and is one of the key reasons for neurological deterioration (Mancuso et al., 2010). CBP50-1 improved the capacity of SOD and CAT (Fig. 5E, F). These results indicated that CBP50-1 might promote the antioxidant system and reduce oxidative damage, and then relieve the symptom of paralysis.

3.9. Polysaccharide CBP50-1 could decrease the Aβ toxicity through the JNK MAPK pathway

The accumulation of Aβ will cause oxidative stress. c-Jun *N*-terminal kinase (JNK) mitogen-activated protein kinase MAPK signaling pathway, one of the MAPK signaling family, acts as a central signaling hub to regulate various important biological processes like movement, and stress resistance (Qu et al., 2020). Moreover, the activated *C. elegans* JNK MAPK can directly phosphorylate DAF-16 which plays an important role in stress resistance (Wolf et al., 2008). CBP50-1 could improve the expression of *jnk-1* and up-regulate the transcription of *daf-16* (Fig. 6).

4. Discussion

Polysaccharide, as a native antioxidant, has been drawn more and more attention due to their low toxicity and stability in the foods or medical field. We optimized the process of hot water extraction of polysaccharide from *C. barometz* rhizome with a yield of 95.9 ± 1.3 mg glucose/g DW. Polysaccharides protect tissues primarily through antioxidant activity organisms. The main mechanism for its antioxidant activity is the riched hydroxyl which could scavenge free radicals. In addition, polysaccharide can reduce oxidative damage through the antioxidant system. CBP50-1 had strong antioxidant activity *in vitro* and could enhance the resistance of *C. elegans* to heat and acute oxidant stress.

The level of Aβ is in dynamic balance, and abnormal Aβ accumulation is one of the main etiologies in AD (Yan et al., 2022). Once the balance was upset, Aβ would accumulate, then a cascade reaction of inflammation, tau phosphorylation, and nerve fiber tangles occurred. These will exacerbate neurotoxicity. Antioxidant-based therapy is a potential pathway to relieve AD in mice (Dumont et al., 2009). *C. elegans* CL4176 expresses human $A\beta_{1\text{-}42}$ in muscle cells when the temperature is higher than 23 °C, which exhibited paralysis symptoms related to AD. CBP50-1 could significantly reduce the accumulation of Aβ and paralysis of *C. elegans* CL4176. The polysaccharide from *Coptis Franch* and *Cyclocarya paliurus* also showed the same function (Li et al., 2018; Lin et al., 2020). To our astonishment, CBP50-1 up-regulated the expression of $A\beta_{1\text{-}42}$, which should not be affected by the non-temperature factor. However, the result of fluorescent staining indicated a decrease in Aβ deposits treated by CBP50-1.

Oxidative stress is dangerous, and it is considered one of the main mechanisms which induce the neurodegenerative cascades of AD. Oxidative stress could lead to both the activation of AD-related pathways and the promotion of AD pathology. Oxidative stress promoted Aβ deposition in APP/PS1 mice, and reduced oxidative damage in mice (Lee et al., 2012; Dumont et al., 2009). CBP50-1 reduced the oxidative injury in CL4176 and N_2 worms, which might explain why CBP50-1 decreased Aβ deposits but up-regulated the expression of $A\beta_{1\text{-}42}$.

The JNK MAPK signaling was proven to regulate stress response in *C. elegans* (Mizuno et al., 2004; Zhao et al., 2015). The *C. elegans* JNK MAPK signaling pathway mainly contains JNK-1, a homolog of human JNK, and two MAP kinase kinases (MEK-1 and JKK-1). MEK-1 and JKK-1 act as activators of JNK. *jnk-1* is expressed in the neurons and could impact *daf-16* directly (Oh et al., 2005). Many natural compounds have proved that activated *daf-16* could enhance the antioxidant activity of *C. elegans* under stress (Abdelfattah et al., 2022; Jabeen et al., 2020; Li et al., 2021). The deposition of Aβ would aggravate the injury in *C. elegans* CL4176, CBP50-1 could affect *jnk-1* to activate *daf-16*, then the antioxidant enzyme activity was increased.

5. Conclusions

In this study, we extracted polysaccharides from the *C. barometz* root. The optimal parameters were ultrasonic power 234 W, liquid to solid ratio 26.5 mL/g, time 70 min, and temperature 68 °C. Under these conditions, the yield of CBP was 95.9 ± 1.3 mg glucose/g DW. CBP50-1 was a neutral polysaccharide with a molecular weight of 61.02 KDa, mainly consisting of glucose and xylose. CBP50-1 had notable antioxidant activities *in vitro*. Furthermore, it relieved the symptom of paralysis induced by the Aβ and enhanced the antioxidant system through the JNK MAPK pathway in the AD model of *C. elegans*. Taking together, CBP50-1 has a potential application in human health industries.

CRediT authorship contribution statement

Zhonghao Zhang: Conceptualization, Methodology, Investigation, Formal analysis, Data curation, Writing – original draft. **Yujin Wang:** Methodology. **Tao Gao:** Methodology. **Zizhong**

Tang: Writing – review & editing. **Lijun Zhou:** Writing – review & editing. **Tao Chen:** Writing – review & editing. **Shiling Feng:** Methodology, Writing – review & editing. **Chunbang Ding:** Writing – review & editing. **Shu Yuan:** Validation. **Ming Yuan:** Conceptualization, Supervision, Resources, Funding acquisition, Project administration, Writing – review & editing.

Declaration of Competing Interest

The authors declare the following financial interests/personal relationships which may be considered as potential competing interests: [Ming Yuan reports financial support was provided by Sichuan Agricultural University.].

Acknowledgments

This work was financially supported by Sichuan Agricultural University.

Appendix A. Supplementary material

Supplementary data to this article can be found online at https://doi.org/10.1016/j.arabjc.2023.104597.

References

Abdelfattah, M.A.O., Dmirieh, M., Ben Bakrim, W., Mouhtady, O., Ghareeb, M.A., Wink, M., Sobeh, M., 2022. Antioxidant and anti-aging effects of *Warburgia salutaris* bark aqueous extract: Evidences from in silico, *in vitro* and *in vivo* studies. J. Ethnopharmacol. 292,. https://doi.org/10.1016/j.jep.2022.115187 115187.

Brookmeyer, R., Abdalla, N., Kawas, C.H., Corrada, M.M., 2018. Forecasting the prevalence of preclinical and clinical Alzheimer's disease in the United States. Alzheimers Dement: J. Alzheimer's Assoc. 14 (2), 121–129. https://doi.org/10.1016/j.jalz.2017.10.009.

Chiang, C.F., Lai, L.S., 2019. Effect of enzyme-assisted extraction on the physicochemical properties of mucilage from the fronds of *Asplenium australasicum* (J. Sm.) Hook. Int. J. Biol. Macromol. 124, 346–353. https://doi.org/10.1016/j.ijbiomac.2018.11.181.

Dumont, M., Wille, E., Stack, C., Calingasan, N.Y., Beal, M.F., Lin, M.T., 2009. Reduction of oxidative stress, amyloid deposition, and memory deficit by manganese superoxide dismutase overexpression in a transgenic mouse model of Alzheimer's disease. FASEB J. 23 (8), 2459–2466. https://doi.org/10.1096/fj.09-132928.

Feng, S.L., Cheng, H.R., Xu, Z., Yuan, M., Huang, Y., Liao, J.Q., Yang, R.W., Zhou, L.J., Ding, C.B., 2018. *Panax notoginseng* polysaccharide increases stress resistance and extends lifespan in *Caenorhabditis elegans*. J. Funct. Foods 45, 15–23. https://doi.org/10.1016/j.jff.2018.03.034.

Folch, J., Ettcheto, M., Petrov, D., Abad, S., Pedrós, I., Marin, M., Olloquequi, J., Camins, A., 2018. Review of the advances in treatment for Alzheimer disease: strategies for combating β-amyloid protein. Neurologia (English Ed). 33 (1), 47–58. https://doi.org/10.1016/j.nrl.2015.03.012.

Gu, J.Y., Li, Q.W., Liu, J., Ye, Z.D., Feng, T., Wang, G., Wang, W. M., Zhang, Y.J., 2020. Ultrasonic-assisted extraction of polysaccharides from *Auricularia auricula* and effects of its acid hydrolysate on the biological function of *Caenorhabditis elegans*. Int. J. Biol. Macromol. 167, 423–433. https://doi.org/10.1016/j.ijbiomac.2020.11.160.

Hamilton, T.R., Mendes, C.M., de Castro, L.S., de Assis, P.M., Siqueira, A.F., Delgado Jde, C., Goissis, M.D., Muino-Blanco, T., Cebrian-Perez, J.A., Nichi, M., Visintin, J.A., Assumpcao, M.E., 2016. Evaluation of lasting effects of heat stress on sperm profile and oxidative status of ram semen and epididymal sperm. Oxid. Med. Cell. Longev. 2016, 1687657. https://doi.org/10.1155/2016/1687657.

Huang, D., Zhang, M.L., Chen, W., Zhang, D.W., Wang, X.L., Cao, H.J., Zhang, Q., Yan, C.Y., 2018. Structural elucidation and osteogenic activities of two novel heteropolysaccharides obtained from water extraction residues of *Cibotium barometz*. Ind. Crop Prod. 121, 216–225. https://doi.org/10.1016/j.indcrop.2018.04.070.

Jabeen, A., Parween, N., Sayrav, K., Prasad, B., 2020. Date (*Phoenix dactylifera*) seed and syringic acid exhibits antioxidative effect and lifespan extending properties in *Caenorhabditis elegans*. Arab. J. Chem. 13 (12), 9058–9067. https://doi.org/10.1016/j.arabjc.2020.10.028.

Jiang, T., Sun, Q., Chen, S., 2016. Oxidative stress: A major pathogenesis and potential therapeutic target of antioxidative agents in Parkinson's disease and Alzheimer's disease. Prog. Neurobiol. 147, 1–19. https://doi.org/10.1016/j.pneurobio.2016.07.005.

Kaldur, T., Kals, J., Ööpik, V., Zilmer, M., Zilmer, K., Eha, J., Unt, E., 2014. Effects of heat acclimation on changes in oxidative stress and inflammation caused by endurance capacity test in the heat. Oxid. Med. Cell. Longev. 2014, 1–8. https://doi.org/10.1155/2014/107137.

Lee, H.P., Pancholi, N., Esposito, L., Previll, L.A., Wang, X.L., Zhu, X.W., Smith, M.A., Lee, H.Y., 2012. Early induction of oxidative stress in mouse model of Alzheimer disease with reduced mitochondrial superoxide dismutase activity. PLoS One 7 (1), e28033.

Li, Y.J., Guan, S.W., Liu, C., Chen, X.H., Zhu, Y.M., Xie, Y.T., Wang, J.B., Ji, X., Li, L.Q., Li, Z.H., Zhang, Y., Zeng, X.Z., Li, M. Q., 2018. Neuroprotective effects of *Coptis chinensis* Franch polysaccharide on amyloid-beta (Aβ)-induced toxicity in a transgenic *Caenorhabditis elegans* model of Alzheimer's disease (AD). Int. J. Biol. Macromol. 113, 991–995. https://doi.org/10.1016/j.ijbiomac.2018.03.035.

Li, N., Li, X., Shi, Y.L., Gao, J.M., He, Y.Q., Li, F., Shi, J.S., Gong, Q.H., 2021. Trilobatin, a component from *Lithocarpus polystachyrus* Rehd., increases longevity in *C. elegans* through activating SKN1/SIRT3/DAF16 signaling pathway. Front. Pharmacol. 12,. https://doi.org/10.3389/fphar.2021.655045 655045.

Lin, C.X., Su, Z.X., Luo, J., Jiang, L., Shen, S.D., Zheng, W.Y., Gu, W.X., Cao, Y., Chen, Y.J., 2020. Polysaccharide extracted from the leaves of *Cyclocarya paliurus* (Batal.) Iljinskaja enhanced stress resistance in *Caenorhabditis elegans* via *skn-1* and *hsf-1*. Int J Biol Macromol. 143, 243–254. https://doi.org/10.1016/j.ijbiomac.2019.12.023.

Liu, Y., Huang, G., 2018. The derivatization and antioxidant activities of yeast mannan. Int. J. Biol. Macromol. 107 (Pt A), 755–761. https://doi.org/10.1016/j.ijbiomac.2017.09.055.

Mancuso, M., Orsucci, D., LoGerfo, A., Calsolaro, V., Siciliano, G., 2010. Clinical features and pathogenesis of Alzheimer's Disease: Involvement of mitochondria and Mmitochondrial DNA. In: Ahmad, S.I. (Ed.), Diseases of DNA Repair. Springer, New York, pp. 34–44.

Mizuno, T., Hisamoto, N., Terada, T., Kondo, T., Adachi, M., Nishida, E., Kim, D.H., Ausubel, F.M., Matsumoto, K., 2004. The *Caenorhabditis elegans* MAPK phosphatase VHP-1 mediates a novel JNK-like signaling pathway in stress response. EMBO J. 23 (11), 2226–2234. https://doi.org/10.1038/sj.emboj.7600226.

Mzoughi, Z., Abdelhamid, A., Rihouey, C., Le Cerf, D., Bouraoui, A., Majdoub, H., 2018. Optimized extraction of pectin-like polysaccharide from *Suaeda fruticosa* leaves: characterization, antioxidant, anti-inflammatory and analgesic activities. Carbohyd Polym. 185, 127–137. https://doi.org/10.1016/j.carbpol.2018.01.022.

Oh, S.W., Mukhopadhyay, A., Svrzikapa, N., Jiang, F., Davis, R.J., Tissenbaum, H.A., 2005. JNK regulates lifespan in *Caenorhabditis elegans* by modulating nuclear translocation of forkhead transcription factor/DAF-16. P Natl Acad Sci USA 102 (12), 4494–4499. https://doi.org/10.1073/pnas.0500749102.

Padurariu, M., Ciobica, A., Lefter, R., Serban, I.L., Stefanescu, C., Chirita, R., 2013. The oxidative stress hypothesis in Alzheimer's disease. Psychiat Danub. 25 (4), 401–409.

Qu, M., Li, D., Zhao, Y., Yuan, Y., Wang, D., 2020. Exposure to low-dose nanopolystyrene induces the response of neuronal JNK MAPK signaling pathway in nematode *Caenorhabditis elegans*. Environ. Sci. Eur. 32 (1), 58. https://doi.org/10.1186/s12302-020-00331-8.

Ribeiro, G., Roehrs, M., Bairros, A., Moro, A., Charão, M., Araújo, F., Valentini, J., Arbo, M., Brucker, N., Moresco, R., Leal, M., Morsch, V., Garcia, S.C., 2011. N-acetylcysteine on oxidative damage in diabetic rats. Drug Chem. Toxicol. 34 (4), 467–474. https://doi.org/10.3109/01480545.2011.564179.

Shang, H.M., Zhao, J.C., Guo, Y., Zhang, H.X., Duan, M.Y., Wu, H. X., 2020. Extraction, purification, emulsifying property, hypoglycemic activity, and antioxidant activity of polysaccharides from comfrey. Ind. Crop Prod. 146,. https://doi.org/10.1016/j.indcrop.2020.112183 112183.

Shi, Y., Wang, X., Wang, N., Li, F.F., You, Y.L., Wang, S.Q., 2020. The effect of polysaccharides from *Cibotium barometz* on enhancing temozolomide-induced glutathione exhausted in human glioblastoma U87 cells, as revealed by (1)H NMR metabolomics analysis. Int. J. Biol. Macromol. 156, 471–484. https://doi.org/10.1016/j.ijbiomac.2020.03.243.

Sun, X., Chen, W.D., Wang, Y.D., 2015. Beta-Amyloid: the key peptide in the pathogenesis of Alzheimer's disease. Front. Pharmacol. 6, 221. https://doi.org/10.3389/fphar.2015.00221.

Teng, C., Qin, P.Y., Shi, Z.X., Zhang, W.Y., Yang, X.S., Yao, Y., Ren, G.X., 2020. Structural characterization and antioxidant activity of alkali-extracted polysaccharides from quinoa. Food Hydrocolloid. 133,. https://doi.org/10.1016/j.foodhyd.2020.106392 106392.

Wang, C.S., Hua, D.H., Yan, C.Y., 2015. Structural characterization and antioxidant activities of a novel fructan from *Achyranthes bidentata* Blume, a famous medicinal plant in China. Ind. Crop Prod. 70, 427–434. https://doi.org/10.1016/j.indcrop.2015.03.051.

Wang, X., Yang, Y., Zou, J., Li, Y., Zhang, X.G., 2022. Chondroitin sulfate E alleviates β-amyloid toxicity in transgenic *Caenorhabditis elegans* by inhibiting its aggregation. Int. J. Biol. Macromol. 209, 1280–1287. https://doi.org/10.1016/j.ijbiomac.2022.04.124.

Wang, X.M., Zhang, Z.S., Zhou, H.C., Sun, X., Chen, X.P., Xu, N.J., 2019. The anti-aging effects of *Gracilaria lemaneiformis* polysaccharide in *Caenorhabditis elegans*. Int. J. Biol. Macromol. 140, 600–604. https://doi.org/10.1016/j.ijbiomac.2019.08.186.

Wolf, M., Nunes, F., Henkel, A., Heinick, A., Paul, R.J., 2008. The MAP kinase JNK-1 of *Caenorhabditis elegans*: location, activation, and influences over temperature-dependent insulin-like signaling, stress responses, and fitness. J. Cell. Physiol. 214 (3), 721–729. https://doi.org/10.1002/jcp.21269.

Xu, W., Zhang, F., Luo, Y., Ma, L., Kou, X., Huang, K., 2009. Antioxidant activity of a water-soluble polysaccharide purified from *Pteridium aquilinum*. Carbohyd. Res. 344 (2), 217–222. https://doi.org/10.1016/j.carres.2008.10.021.

Yan, N.N., Zhang, H.F., Zhang, Z.H., Zhang, H.Q., Zhou, L.J., Chen, T., Feng, S.L., Ding, C.B., Yuan, M., 2022. The extraction, antioxidant and against β-amyloid induced toxicity of polyphenols from *Alsophila spinulosa* leaves. Arab. J. Chem. 15, (4). https://doi.org/10.1016/j.arabjc.2022.103707 103707.

Yen, P.L., How, C.M., Hsiu-Chuan Liao, V., 2021. Early-life and chronic exposure to di(2-ethylhexyl) phthalate enhances amyloid-β toxicity associated with an autophagy-related gene in *Caenorhabditis elegans* Alzheimer's disease models. Chemosphere 273,. https://doi.org/10.1016/j.chemosphere.2020.128594 128594.

Yu, N.X., Wang, X.Y., Ning, F.J., Jiang, C.J., Li, Y.B., Peng, H.L., Xiong, H., 2019. Development of antibacterial pectin from *Akebia trifoliata* var. australis waste for accelerated wound healing. Carbohyd Polym. 217, 58–68. https://doi.org/10.1016/j.carbpol.2019.03.071.

Zhang, X.C., Nishida, H., 2013. Cibotiaceae. In: Wu, Z.Y., Raven, P. H., Hong, D.Y. (Eds.), Flora of China. Science Press, Beijing, Missouri Botanical Garden Press, St. Louis, pp. 132-133.

Zhang, Y., Mi, D.Y., Wang, J., Luo, Y.P., Yang, X., Dong, S., Ma, X. M., Dong, K.Z., 2018. Constituent and effects of polysaccharides isolated from *Sophora moorcroftiana* seeds on lifespan, reproduction, stress resistance, and antimicrobial capacity in *Caenorhabditis elegans*. Chin. J. Nat. Med. 16, 252–260. https://doi.org/10.1016/S1875-5364(18)30055-4.

Zhao, Y.Q., Hu, W.C., Zhang, H.F., Ding, C.B., Huang, Y., Liao, J. Q., Zhang, Z.W., Yuan, S., Chen, Y.E., Yuan, M., 2019. Antioxidant and immunomodulatory activities of polysaccharides from the rhizome of *Dryopteris crassirhizoma* Nakai. Int. J. Biol. Macromol. 130, 238–244. https://doi.org/10.1016/j.ijbiomac.2019.02.119.

Zhao, Y., Wu, Q., Wang, D., 2015. A microRNAs–mRNAs network involved in the control of graphene oxide toxicity in *Caenorhabditis elegans*. RSC Adv. 5 (112), 92394–92405. https://doi.org/10.1039/C5RA16142H.

Zheng, L., Roberg, K., Jerhammar, F., Marcusson, J., Terman, A., 2006. Oxidative stress induces intralysosomal accumulation of Alzheimer amyloid beta-protein in cultured neuroblastoma cells. Ann. N.Y. Acad. Sci. 1067, 248–251. https://doi.org/10.1196/annals.1354.032.

Zheng, Y., Xie, Q.X., Wang, H., Hu, Y.J., Ren, B., Li, X.F., 2020. Recent advances in plant polysaccharide-mediated nano drug delivery systems. Int. J. Biol. Macromol. 165, 2668–2683. https://doi.org/10.1016/j.ijbiomac.2020.10.173.

Zhou, W.W., Lu, S., Su, Y.J., Xue, D., Yu, X.L., Wang, S.W., Zhang, H., Xu, P.X., Xie, X.X., Liu, R.T., 2014. Decreasing oxidative stress and neuroinflammation with a multifunctional peptide rescues memory deficits in mice with Alzheimer disease. Free Radical Bio Med. 74, 50–63. https://doi.org/10.1016/j.freeradbiomed.2014.06.013.